

SparseOccVLA: Bridging Occupancy and Vision-Language Models via Sparse Queries for Unified 4D Scene Understanding and Planning

Chenxu Dang^{1,2,3*} Jie Wang² Guang Li² Zhiwen Hou² Zihan You³ Hangjun Ye²
 Jie Ma¹ Long Chen^{2†} Yan Wang^{3†}

¹Huazhong University of Science and Technology

²Xiaomi EV ³Institute for AI Industry Research (AIR), Tsinghua University

<https://msundyy.github.io/SparseOccVLA>

Abstract

*In autonomous driving, Vision Language Models (VLMs) excel at high-level reasoning, whereas semantic occupancy provides fine-grained details. Despite significant progress in individual fields, there is still no method that can effectively integrate both paradigms. Conventional VLMs struggle with token explosion and limited spatiotemporal reasoning, while semantic occupancy provides a unified, explicit spatial representation but is too dense to integrate efficiently with VLMs. To address these challenges and bridge the gap between VLMs and occupancy, we propose **SparseOccVLA**, a novel vision-language-action model that unifies scene understanding, occupancy forecasting, and trajectory planning powered by **sparse occupancy queries**. Starting with a lightweight Sparse Occupancy Encoder, SparseOccVLA generates compact yet highly informative sparse occupancy queries that serve as the single bridge between vision and language. These queries are aligned into the language space and reasoned by the LLM for unified scene understanding and future occupancy forecasting. Furthermore, we introduce an LLM-guided Anchor-Diffusion Planner featuring decoupled anchor scoring and denoising, as well as cross-model trajectory-condition fusion. SparseOccVLA achieves a 7% relative improvement in CIDEr over the state-of-the-art on OmniDrive-nuScenes, a 0.5 increase in mIoU score on Occ3D-nuScenes, and sets state-of-the-art open-loop planning metric on nuScenes benchmark, demonstrating its strong holistic capability.*

1. Introduction

In recent years, Vision-Language Models (VLMs)[4, 18, 19, 24, 33, 43] have witnessed remarkable progresses in end-to-end autonomous driving[12, 15, 16, 36]. With strong

understanding and reasoning capabilities, VLMs are expected to handle long-tail cases and offer interpretability.

However, conventional VLMs pretrained on web-scale 2D images inherently lack temporal-spatial awareness[9, 53]. Autonomous driving systems are required to process multi-view, multi-frame video streams for comprehensive perception, which imposes an astronomical number of vision tokens and impedes the deployment of VLMs. Some approaches[3, 44] adopt Q-Former[19] to compress tokens, but their indiscriminate global cross-attention inevitably discards image details, resulting in suboptimal performance. Moreover, multi-view cameras introduce view ambiguity[17], which remains a significant challenge.

Recent studies[57, 58] project multi-view images into Bird’s-Eye View (BEV). Although alleviating view ambiguity, the dense BEV still incurs an enormous number of tokens (e.g., a 50×50 BEV map corresponds to 2,500 tokens). In practice, due to inherent sparsity of road scenes, more than 80% of BEV tokens are invalid, revealing the inefficiency of BEV representation. Moreover, the compression of BEV inevitably sacrifices spatial details, making it difficult to handle unstructured scenarios.

Compared to BEV, semantic occupancy offers more comprehensive and granular representations[39], and has attracted increasing attention[26, 30, 45, 50] since its introduction. Nevertheless, occupancy and VLMs have long evolved separately, with no effective integration achieved to fully exploit the strengths of both. The key challenge lies in the inherently dense and low-level nature of occupancy, which hinders its alignment with LLMs. Some early attempts[46, 48] discretized occupancy ground truth and embedded it via VQ-VAE[40], but such paradigms separate understanding from perception and discards critical non-geometric visual cues—such as traffic lights, lane markings and signs. Recent OccVLA[27] employs occupancy supervision to enhance VLMs, yet still relies on visual tokens and thus inherits the limitations of conventional VLMs. Overall,

*Work done during the internship at Xiaomi EV and AIR.

†Corresponding Authors.

occupancy remains marginal within VLMs, and how to integrate them effectively has long perplexed the community.

Recently, sparse representations have achieved great success in occupancy perception[26, 42] and forecasting[5], providing a promising avenue for integrating occupancy with VLMs. In response, we propose SparseOccVLA. Relying solely on sparse occupancy queries, SparseOccVLA effectively bridging low-level occupancy perception with high-level scene understanding.

SparseOccVLA starts with a Sparse Occupancy Encoder, where learnable query embeddings progressively interact with multi-view, multi-scale image features through stacked encoding layers, ultimately generating compact occupancy queries (only a few hundred). These queries are aligned with the language space, serving as the sole bridge between visual input and the LLM. We also specifically design token-level distillation and global query mechanism to facilitate the cross-modal alignment. The resulting multi-modal tokens reasoned by a unified LLM are utilized in parallel for scene understanding and future occupancy forecasting.

To investigate the capability of our sparse occupancy-oriented VLM in downstream planning, we design an LLM-guided Anchor-Diffusion planner where the LLM is prompted to assign high-level scores to trajectory anchors. A diffusion decoder then allows text-level instruction features, occupancy queries and ego states to interact alternately with noised trajectories, enabling cross-modal trajectory-condition fusion and noisy prediction. This decoupling exploits the complementary strengths of LLMs for decision-making and diffusion models for regression.

Extensive experiments demonstrate the strong holistic capability of SparseOccVLA. Notably, it attains a CIDEr score of 0.795 on the OmniDrive-nuScenes[44] benchmark, surpassing the recent HERMES[58] by 7%. For occupancy forecasting, our method outperforms the recent SparseWorld[5] by up to 0.51 in average mIoU. Moreover, our planner establishes new SOTA performance on open-loop metrics in the nuScenes dataset.

We summarize our key contributions as follows:

- To the best of our knowledge, SparseOccVLA is the first bonafide occupancy-oriented end-to-end VLA model that unifies understanding, forecasting and planning.
- The compact and information-rich sparse queries effectively link occupancy representation with scene understanding, serving as a novel vision-language connector superior to conventional ones for autonomous driving.
- We design an LLM-guided anchor diffusion planner, which simultaneously leverages the strengths of both LLMs and diffusion models.
- SparseOccVLA achieves strong performance in scene understanding, occupancy prediction, and planning tasks.

2. Related Work

2.1. VLM for Autonomous Driving

Early end-to-end planners[12, 16, 36, 51] are generally regarded as black-boxes, lacking interpretability and struggling to handle long-tail scenarios. In recent years, vision-language models[18, 24, 43] (VLMs) have been widely adopted for scene understanding[14, 34, 44] and chain-of-thought (CoT)[13, 28, 31] reasoning. Subsequent works sought to integrate VLMs with end-to-end planners into dual-system architectures[3, 17, 38].

To align images with LLMs, some methods[17, 28, 54] employ a standard MLP projection, which can produce excessively large and cumbersome visual tokens. Others[3, 7, 31, 44] employ a Q-Former[19] mechanism, which utilizes a small number of queries to attend to the entire image for token compression. Such indiscriminate global interaction, however, inevitably results to the loss of rich semantic details. To enhance the spatial understanding capability of VLMs, recent approaches[57, 58] attempt to project multi-view images into the BEV space before feeding them into LLMs. However, BEV representations suffer from uneven information distribution.

2.2. Occupancy for Autonomous Driving

Semantic occupancy provides a more detailed and fine-grained spatial representation[39], particularly excelling at modeling irregular elements. Early studies mainly focused on occupancy perception[30, 45, 50, 52] and static forecasting[29, 47]. Occupancy-based world models to autoregressively forecast future occupancies and trajectories. To address the intrinsic density of occupancy, several sparse approaches[5, 26, 42] have been proposed, enhancing their applicability in downstream tasks.

2.3. Combination of occupancy and VLMs

In the era of large language model, some works[46, 48] attempted to discretize occupancy ground truth and embed via VQ-VAE[40] for LLM understanding. However, such designs isolate the LLM from the perception, completely discarding non-geometric visual cues—such as traffic lights and lane markings—that are critical for driving decisions. The concurrent OccVLA[27], leverages occupancy supervision to enhance VLA, yet it still relies on visual tokens.

Despite the remarkable success of both occupancy and VLMs, to the best of our knowledge, no existing work has effectively integrated them. This is primarily due to occupancy’s dense nature creating a significant modality gap. A more detailed analysis is included in the supplementary material, which we encourage readers to consult.

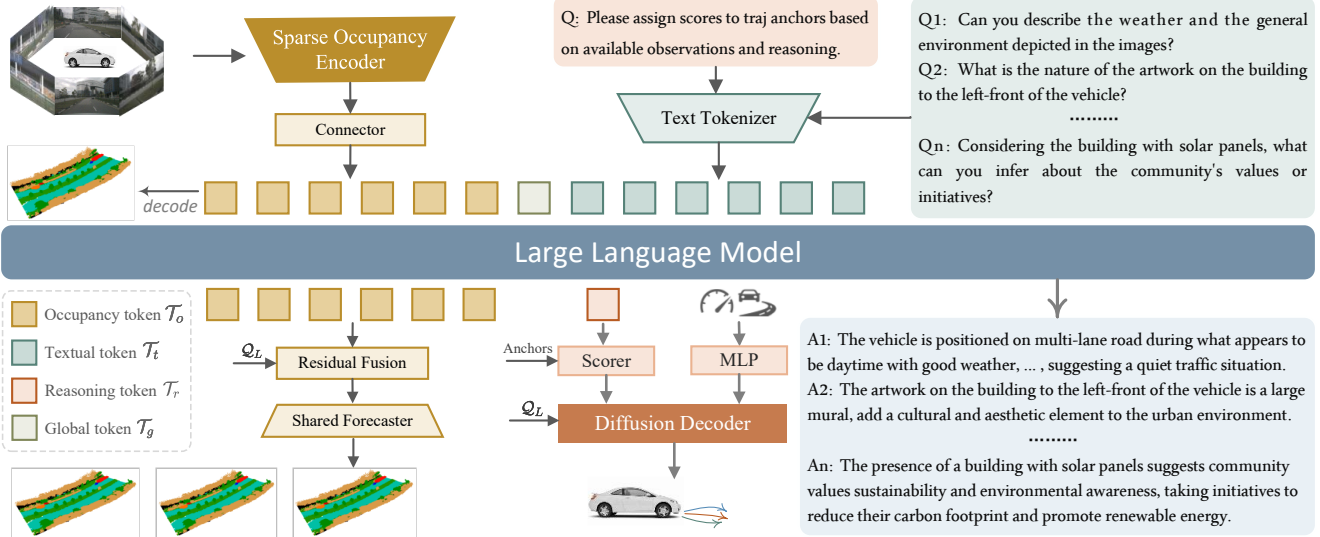


Figure 1. The overview of SparseOccVLA, which is based on sparse occupancy queries, with a large language model serving as a unified token processor to simultaneously perform scene understanding, occupancy forecasting, and trajectory planning.

3. Method

The overall architecture of our SparseOccVLA is illustrated in Fig. 1. The inputs include multi-view, multi-frame images, textual instructions, and ego-state information. The images are processed by a Sparse Occupancy Encoder (Sec. 3.1), which generates a set of sparse occupancy queries. With no visual tokens, only aligned occupancy tokens are fed into the LLM (Sec. 3.2) for unified understanding and forecasting. In (Sec. 3.3), we elaborate on the LLM-guided Anchor-Diffusion Planner for cross-modal fusion with trajectory anchors.

3.1. Sparse Occupancy Encoder

As shown in Fig. 2, Sparse Occupancy Encoder takes as input multi-view, multi-frame images $\mathcal{I} = \{I_{v,f}|v = 1, \dots, V; f = 1, \dots, F\}$. We randomly initialize a set of sparse occupancy query embeddings $\mathcal{Q}_0 = \{\mathbf{q}_i \in \mathbb{R}^D\}_{i=1}^N$, along with their 3D positions $\mathcal{P}_0 = \{\mathbf{p}_i \in \mathbb{R}^3\}_{i=1}^N$. Here, F , V , N , and D represent the number of image frames, camera views, queries, and feature dimension, respectively.

We employ a lightweight image encoder to extract multi-scale features for each image. The initial occupancy embeddings $[\mathcal{Q}_0, \mathcal{P}_0]$ are fed into a stack of L encoding layers. The encoding layer follows the design of SparseBEV[25], consisting of feature sampling, adaptive fusion, spatial-aware multi-head self-attention (Spatial-aware MHSA), and a FFN. This design effectively extracts cross-frame and multi-scale features and has been widely adopted in recent works[5, 26, 42]. Following each layer, the queries are decoded into a set of occupancy points while updating their coordinates consequently. We progressively increase the

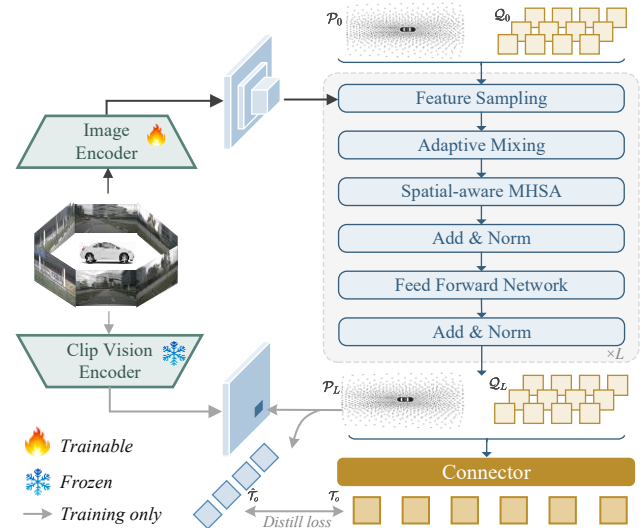


Figure 2. Illustration of the Sparse Occupancy Encoder, where the distillation branch (indicated by gray) is removed during inference.

number of points predicted across layers, enabling a coarse-to-fine occupancy encoding. The point set \mathcal{P}_l output from each layer is supervised with Chamfer Distance (CD):

$$CD(\mathcal{P}_l, \mathcal{G}) = \sum_{\mathbf{p} \in \mathcal{P}_l} \min_{\mathbf{g} \in \mathcal{G}} \|\mathbf{p} - \mathbf{g}\|_2^2 + \sum_{\mathbf{g} \in \mathcal{G}} \min_{\mathbf{p} \in \mathcal{P}_l} \|\mathbf{p} - \mathbf{g}\|_2^2, \quad (1)$$

where $l = 1, 2, \dots, L$ and \mathcal{G} denotes the sparsified ground-truth point set. The semantic output of each predicted point is supervised using the focal loss with respect to the label of its matched ground-truth point.

The outputs \mathcal{Q}_L and \mathcal{P}_L from the final L -th encoding layer are combined and aligned to the LLM space through a lightweight connector (implemented as an MLP):

$$\mathcal{T}_o = \text{MLP}(\mathcal{Q}_L + \text{PE}(\mathcal{P}_L)), \quad (2)$$

where, PE denotes positional encoding. The aligned representations \mathcal{T}_o , referred to as occupancy tokens, inherently encode geometric and semantic cues in a highly compact form, allowing them to serve as a complete substitute for conventional image tokens for LLM understanding.

Feature-level Distillation In our early exploration, we observed that the LLM exhibited an extremely high initial loss, which led to slow convergence or even training collapse. We attribute this to the large gap between the low-level occupancy representation and the high-level language space. This is particularly exacerbated by the sparsity and disorder of the occupancy queries.

To address this issue, we design a feature-level distillation loss to assist training. As in Fig. 2, when training the occupancy encoder, we simultaneously extract single-frame, single-scale feature from a pretrained and frozen CLIP[33] Vision Encoder. The occupancy tokens \mathcal{T}_o are projected via their 3D coordinates and to sample the teacher features $\hat{\mathcal{T}}_o$ via interpolation. A cosine similarity loss is computed between \mathcal{T}_o and $\hat{\mathcal{T}}_o$ to encourage alignment.

However, we observe that overly strict constraints significantly hinders the occupancy encoder learning. Therefore, before computing the loss, we apply independent Layer-Norm layers to \mathcal{T}_o and $\hat{\mathcal{T}}_o$, which normalize their mean and variance and align only their relative feature shapes. Moreover, the learnable γ and β further mitigate the strength of the constraint. Consequently, the final distillation loss is formulated as:

$$\mathcal{L}_{\text{distill}} = 1 - \text{cosine}(\text{Norm1}(\mathcal{T}_o), \text{Norm2}(\hat{\mathcal{T}}_o)). \quad (3)$$

3.2. Unified Large Language Model

Inputs As discussed in Sec. 3.1, the occupancy tokens preserve rich details but focus only on local regions, lacking a global representation. To mitigate this limitation, we introduce a small set of learnable global scene tokens \mathcal{T}_g that query all occupancy tokens \mathcal{T}_o via cross-attention:

$$\mathcal{T}_g = \text{Cross-Attn}(\mathcal{T}_g, \mathcal{T}_o, \mathcal{T}_o). \quad (4)$$

The language instructions are tokenized as textual tokens \mathcal{T}_t . Ultimately, the combined tokens $\mathcal{T}_{\text{all}} = [\mathcal{T}_o, \mathcal{T}_g, \mathcal{T}_t]$ are sequentially fed into the LLM for processing and joint execution of downstream understanding and forecasting.

Understanding Following prior works[44, 58], our SparseOccVLA autoregressively generates answers based

on perception-level tokens and textual prompts, describing the driving environment, localizing key objects, and making high-level driving decisions. The LLM is supervised using the standard maximum likelihood estimation (MLE) loss:

$$\mathcal{L}_{\text{LM}} = - \sum_{n=1}^N \log P_{\theta}(y_t | y_{<n}), \quad (5)$$

where N denotes the token length.

For simplicity, we employ causal attention over all tokens. It is noteworthy that, unlike visual tokens that are structured, occupancy tokens are essentially point clouds, which are sparse and unordered, thus the LLM must rely solely on their 3D coordinates to infer spatial topology. We observe that manually permuting the order of occupancy tokens or using bidirectional masking does not promote overall performance, which is counterintuitive, but also demonstrates that the LLM can understand the scene relying solely on token positions, enhancing overall robustness.

Forecasting Inspired by [58], we consider that occupancy tokens \mathcal{T}_o after LLM reasoning, denoted as \mathcal{T}'_o , carry linguistic cues and a global context, while the occupancy queries \mathcal{Q}_L retain low-level details, their combination may enable complementary interaction. Consequently, we design a simple residual fusion linear layer to merge them:

$$\hat{\mathcal{Q}}_o = \text{MLP}([\mathcal{T}'_o, \mathcal{Q}_L]). \quad (6)$$

Here, $\hat{\mathcal{Q}}_o$ and \mathcal{Q}_L share the same dimension D . Furthermore, $\hat{\mathcal{Q}}_o$ are progressively augmented with 4D embeddings and ego-vehicle states:

$$\hat{\mathcal{Q}}_o^t = \hat{\mathcal{Q}}_o + \text{embed}(X, Y, Z, t) + \text{Ego}, \quad (7)$$

where X, Y, Z denote the 3D coordinates of queries, and $t = 1, 2, \dots, T$, T represents the horizon to be forecasted. A shared forecaster is employed to recursively forecast the future occupancy frame by frame, which is supervised with the corresponding frame's occupancy ground truth, consistent with Sec. 3.1.

3.3. LLM-guided Anchor-Diffusion Planner

Recently, anchor-based diffusion planner[21] has demonstrated significant advantages, where diffusion is applied to slightly perturb anchors, followed by per-anchor scoring and denoising. However, these methods still lack integration with LLM reasoning and guidance.

To bridge this gap, we propose an LLM-guided anchor-diffusion planner. Following [21], we first apply K-means clustering on the training trajectories to obtain K anchor trajectories $\{\mathbf{a}_k\}_{k=1}^K$, which naturally exhibit significant diversity. As in Fig. 1, We prompt the LLM to generate reasoning tokens \mathcal{T}_r , followed by a scorer that assigns scores to

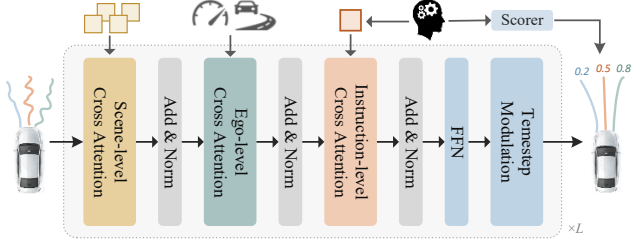


Figure 3. The architecture of Diffusion Decoder.

anchors based on contextual understanding, reasoning, and ego state. The scorer is supervised with BCE Loss, where the anchor closest to the ground-truth is regarded as the positive sample and the others as negatives.

We follow the standard DDIM[35] noising and denoising strategy to optimize the anchors. During training, Gaussian noise is added to all anchors:

$$\tau_k^i = \sqrt{\bar{\alpha}^i} \mathbf{a}_k + \sqrt{1 - \bar{\alpha}^i} \boldsymbol{\epsilon}, \quad \boldsymbol{\epsilon} \sim \mathcal{N}(0, \mathbf{I}), \quad (8)$$

where i denotes the noising step. The noised anchors $\{\tau_k\}_{k=1}^K$ are jointly fed into a conditional diffusion decoder to regress the clean trajectories directly. Only the positive anchor is supervised using $L1$ loss. During inference, the anchor trajectories are randomly noised and iteratively denoised, and the denoised result corresponding to the anchor selected by the LLM is chosen as the final trajectory.

As shown in Fig. 3, the diffusion decoder encodes the noised trajectories and employ stacked cross-attention layers to sequentially attend to (1) scene-level occupancy queries Q_0 , (2) the encoded ego state, and (3) the LLM-generated tokens for decision. This multi-modal and cross-level fusion enables the planner to jointly reason over geometric perception, dynamic context, and high-level semantics, thereby improving the rationality and consistency of the generated trajectories. Here, we completely discard BEV features, boxes and maps, only occupancy queries serving as perceptual input. A feed-forward network (FFN) and a timestep modulation layer are applied to enhance temporal conditioning and representation stability.

4. Experiments

4.1. Datasets and Benchmarks

We benchmark our model on the public nuScenes dataset[2], which contains 700/150/150 scenes for training, validation, and testing. Each scene provides six camera views and spans 20 seconds with 2 Hz key frames.

For understanding, we adopt OmniDrive-nuScenes[2] benchmark, which provides detailed captions and VQA pairs generated by GPT-4V. Following prior works[44, 58], we report METEOR[1], CIDEr[41], and ROUGE[23] metrics. For occupancy forecasting task, we employ Occ3D-

nuScenes[37], which divides the 3D space into a $200 \times 200 \times 16$ voxel grid with a 0.4m resolution. It provides high-quality dense semantic annotations covering 18 categories (including free class). We evaluate SparseOccVLA's forecasting performance through the mean Intersection over Union (mIoU) over the future 3 seconds. To ensure a fair comparison, we do not utilize camera mask while computing the mIoU. For the planning task, the evaluation metrics include open-loop L2 error and collision rate over future 3s. We compute understanding and planning scores over the full dataset. For the mIoU forecasting, the first five and last seven frames of each scene are excluded, consistent with prior works[20, 56].

4.2. Implementation Details

Model Details We adopt ResNet-50[10] to extract multi-scale features from multi-view images of size 256×704 , and CLIP-336[33] vision encoder for distillation. For the occupancy encoder, we randomly initialize 600 queries and 6 encoding layers, where each query generates (2, 4, 16, 32, 56, 112) points across layers. The feature dimension of occupancy query is 1024. We use Vicuna-7B[55] as our LLM, which consists of 32 attention layers with a token feature dimension of 4096. The number of global queries is set to 12. For planning, we cluster 18 anchor trajectories and perform 2 denoising steps for refinement.

Training Details Our training process consists of three stages. In stage 1, we train the sparse occupancy encoder and the connector with occupancy loss and the distillation loss. In stage 2, we freeze the visual encoder and train the connector, global queries, and downstream forecasting and planning modules. In stage 3, we train all parameters except for the LLM, which is fine-tuned using the LoRA[11], and the LoRA rank r and scaling factor α are set to 128 and 16, respectively. All training stages are conducted on 8 NVIDIA H20 GPUs with a total batch size of 16. We set the base learning rate to $2e-4$ and adopt the AdamW optimizer with a cosine decay schedule to facilitate convergence. The three stages are trained for 36, 6, and 12 epochs, respectively. Each stage directly loads the weights from the previous one. More details about the model architecture and training settings can be found in our appendix.

4.3. Main Results

Scene Understanding As shown in the left part of Tab. 1, SparseOccVLA significantly outperforms existing state-of-the-art models on Omnidrive-nuScenes[44] across all three metrics, with a notable 7% gain CIDEr compared to HERMES[58]. Notably, methods based on BEV or image tokens require a large number of tokens, whereas our lightweight version achieves strong performance with only 300 occupancy tokens, demonstrating the high information

Table 1. Performance comparison of SparseOccVLA with current state-of-the-art methods for scene understanding (left) and occupancy prediction (right). The best results are highlighted in **bold**. "Token" refers to the number of tokens representing image information.

Left Table: Understanding				Right Table: Forecasting					
Method	Token	Understanding \uparrow			Method	mIoU \uparrow			
		METEOR	ROUGE	CIDEr		1s	2s	3s	Avg
LLaVA-OV[24]	>1500	-	0.221	0.284	OccWorld[56]	11.55	8.10	6.22	8.62
OmniDrive-BEV[44]	2500	0.356	0.278	0.595	OccLLaMA[46]	10.34	8.66	6.98	8.66
OmniDrive[44]	512	0.380	0.326	0.686	PreWorld[20]	12.27	9.24	7.15	9.55
HERMES-p[58]	2500	0.380	0.323	0.726	Occ-LLM[48]	11.28	10.21	9.13	10.21
HERMES[58]	2500	0.384	0.327	0.741	SparseWorld[5]	14.93	13.15	11.51	13.20
SparseOccVLA	300	0.384	0.333	0.762	SparseOccVLA	15.36	13.12	11.42	13.30
SparseOccVLA	600	0.388	0.337	0.796	SparseOccVLA	15.86	13.54	11.72	13.71

Table 2. Comparison of SparseOccVLA with different types of planning models on open-loop planning performance in nuScenes. The best results are highlighted in **bold**.

Method	Type	Auxiliary Supervision	L2 (m) \downarrow				Collision Rate (%) \downarrow			
			1s	2s	3s	Avg.	1s	2s	3s	Avg.
UniAD[12]	End to End	Map & Box & Motion & Occupancy	0.20	0.42	0.75	0.46	0.02	0.25	0.84	0.37
VAD-Base[16]	End to End	Map & Box & Motion	0.17	0.24	0.60	0.37	0.04	0.27	0.67	0.33
OccWorld[56]	World model	3D Occupancy	0.39	0.73	1.18	0.77	0.11	0.19	0.67	0.32
PreWorld [20]	World model	2D Label & 3D Occupancy	0.22	0.30	0.40	0.31	0.21	0.66	0.71	0.53
SparseWorld [5]	World model	3D-Occ	0.19	0.25	0.36	0.27	0.11	0.29	0.46	0.29
HERMES-p [58]	VLM	QA & Lidar	0.16	0.32	0.59	0.36	0.00	0.14	0.82	0.32
Omnidrive [44]	VLM	QA	0.14	0.29	0.55	0.33	0.00	0.13	0.78	0.30
OpenDriveVLA[57]	VLA	Map & Box & Motion & QA	0.15	0.31	0.55	0.33	0.00	0.22	0.55	0.25
OccVLA [27]	VLA	QA & 3D-Occ	0.18	0.26	0.40	0.28	-	-	-	-
SparseOccVLA	Unified	QA & 3D-Occ	0.14	0.22	0.32	0.23	0.03	0.12	0.41	0.19

density. In contrast, OmniDrive-base[44], which leverages a Q-Former to compress tokens, suffers from indiscriminate global querying that discards much fine-grained details, resulting in suboptimal performance.

Occupancy Forecasting As shown in the right part of Tab. 1, SparseOccVLA consistently achieves SOTA performance. With the assistance of the large language model, its occupancy forecasting is markedly improved compared to the similarly sparse SparseWorld[5], with an average future 3s mIoU increase of 0.51.

Trajectory Planning As presented in Tab. 2, we compare SparseOccVLA against end-to-end methods, VLA, and world models. The results demonstrate that SparseOccVLA consistently outperforms all competitors. We argue that with LLM guidance, decoupling anchor scoring

from noisy regression allows the model to fully exploit the strengths of both LLMs and diffusion. The strong performance in planning further demonstrates the representational power of sparse occupancy queries, which can serve as the sole perception-level input.

4.4. Ablation Studies

In this section, we provide detailed ablation studies to investigate the contribution of each component and design. Limited by space, we provide additional experimental results in the appendix, including results on nuScenes-QA[32], normalization layers for distillation as well as the effects of the number of global queries and image sweeps.

Effect of the Occupancy We first investigate the impact of occupancy modeling on overall understanding ability. As shown in 2th row of Tab. 3, when the occupancy super-

Table 3. Ablation studies about different components on the understanding metrics and the average mIoU over the future 3s.

Method	CIDEr	METEOR	ROUGE	mIoU
w/o Occ Encoder	0.712	0.363	0.317	-
w/o Position Encoding	-	-	-	-
w/o Global Queries	0.758	0.378	0.327	13.50
w/o Residual-Query	0.764	0.377	0.329	13.12
w/o Residual-Token	0.788	0.382	0.333	13.21
Base model	0.792	0.384	0.334	13.65

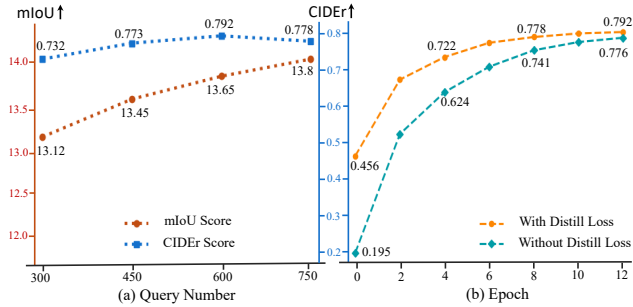


Figure 4. Ablation study on the number of queries (a), and the distillation loss (b).

vision is removed and only the textual loss is preserved, the occupancy encoder essentially degenerates into a Q-Former-like module, except that the queries attend to local rather than global features. We observe a significant drop (-0.8) in CIDEr, indicating that the occupancy loss serves as an effective regularizer, endowing the queries with explicit geometric and semantic priors for better LLM understanding. Without it, the heterogeneous and sparse supervision from the LLM alone struggles to achieve effective alignment between the visual encoder and the language model. Furthermore, as shown in the 3th row of Tab. 3, when the 3D position encoding is removed during the alignment from occupancy queries to occupancy tokens, the model fails to converge. This is because, without explicit positional information, the LLM perceives the queries as an unordered and unstructured set of tokens, making it impossible to capture the underlying spatial topology.

Analysis of global queries As shown in row 4 of Tab. 3, introducing global queries yields a 0.34 improvement in the CIDEr score, confirming our hypothesis that occupancy queries primarily focus on local details and lack scene-level understanding. The global queries effectively complement this limitation, providing a more holistic representation.

Residual Fusion and Uniformity Analysis As shown in row 5 of Tab. 3, removing the residual fusion of occu-

Table 4. Ablation study on the planning module. We report L2 distance error and collision rate at 1s, 2s, 3s, and their averages.

Model Setting	L2 (m)			Coll. Rate (%)		
	1s	2s	3s	1s	2s	3s
w/o LLM Scoring	0.17	0.28	0.41	0.03	0.25	0.49
w/o Traj-Reason Fusion	0.14	0.26	0.35	0.04	0.19	0.41
w/o Traj-Scene Fusion	0.15	0.28	0.38	0.04	0.23	0.46
w/o Traj-Ego Fusion	0.22	0.35	0.68	0.07	0.29	0.65
Base Model	0.14	0.22	0.30	0.03	0.16	0.39

pancy query causes a noticeable drop in CIDEr (-0.28). We hypothesize that this is because the queries must simultaneously align with the LLM while preserving their original perception-level features, thus increasing the LLM’s learning burden. In row 6, when the occupancy tokens are removed, the LLM becomes decoupled from forecasting and is only responsible for text-level understanding. In this case, the language metrics remain similar to the standard model, but the mIoU remains low (-0.44). This indicates that LLM understanding facilitates occupancy forecasting, while the reverse effect is weaker. By effectively fusing high-level occupancy tokens with low-level occupancy queries, SparseOccVLA leverages the complementary strengths of both, highlighting the advantage of unified modeling.

Effect of Query Number As shown in the blue curve on the Fig. 4(a), SparseOccVLA exhibits insensitivity to the number of queries. Even with only 300 queries, it still achieves a CIDEr score of 0.732, demonstrating its high information density and robust scene understanding capability. We also observe a decline in CIDEr when the number of queries increases, which we attribute to the increased disorder that imposes a heavier interpretative burden on the LLM. In contrast, as indicated by the red curve, the mIoU shows a consistent positive correlation with the number of queries due to its low-level nature.

Effect of the Distillation Loss As shown in the Fig. 4(b), applying the distillation loss during the training of the Occupancy Encoder immediately yields an initial CIDEr score of 0.456 and consistently outperforms the counterpart without distillation. Although the final performance of both models eventually converges, introducing the distillation loss significantly accelerates convergence and enhances training stability. We observe that removing the distillation loss often causes gradient explosion and instability, particularly with a large number of queries, while its inclusion effectively mitigates such failures.

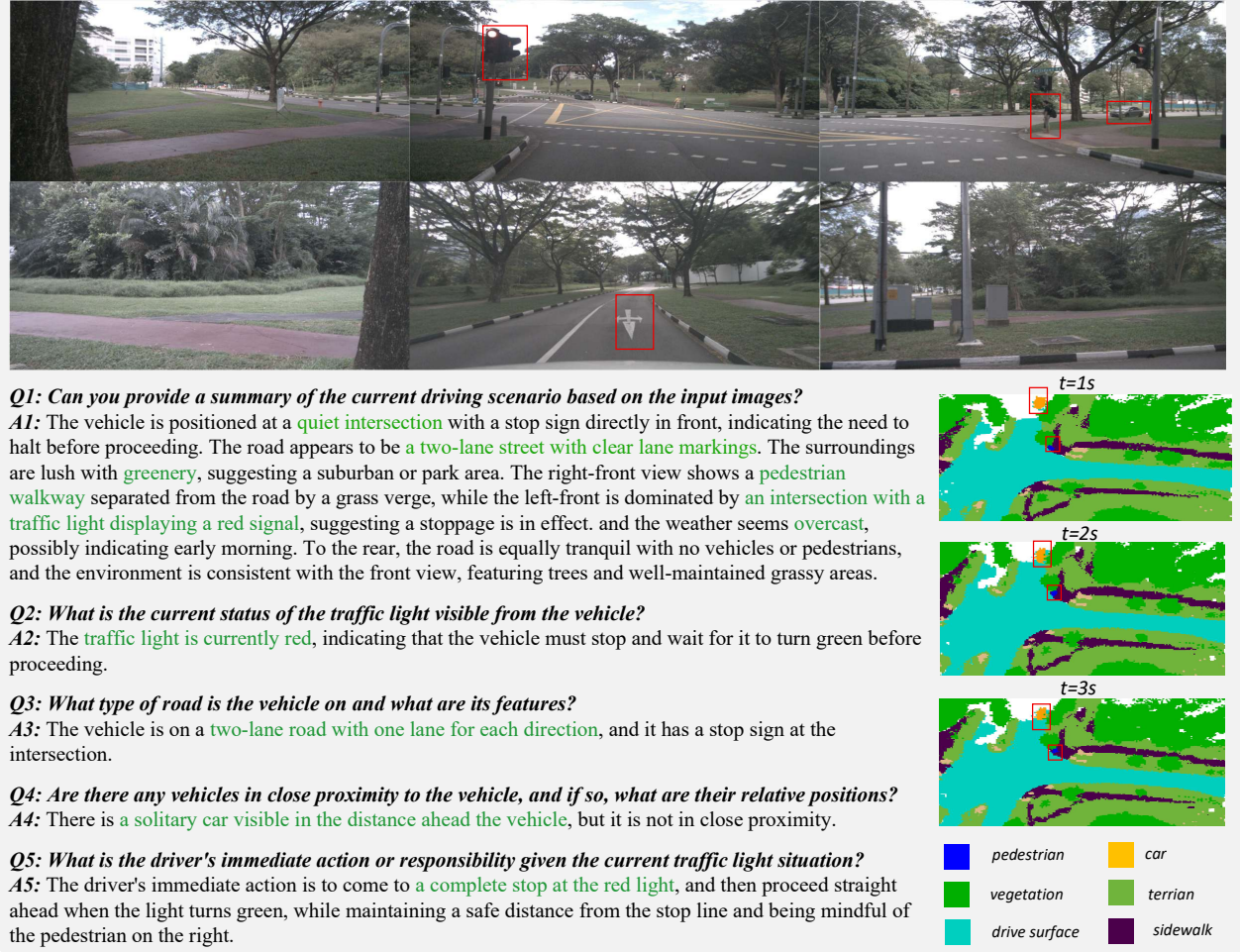


Figure 5. Qualitative results of SparseOccVLA for scene understanding and occupancy forecasting.

Effect of LLM-guided Planning As shown in Tab. 4, row 3, removing the LLM-guided scoring—leaving the planner to independently score while regressing anchor noise, results in a notable degradation in both L2 distance and collision rate metrics. We attribute this to SparseOccVLA effectively degenerating into a purely end-to-end planner, lacking a global perspective and imposing a greater optimization burden on the model. LLMs, in contrast, offer robust high-level scene understanding and reasoning capacity.

Effect of Multi-Modal Fusion As shown in rows 4–6 of Tab. 3, fusing the trajectory embeddings with language instructions, scene context, and ego-state reduces the average L2 error by 0.03m, 0.05m, and 0.19m, respectively. This demonstrates the consistent benefits of cross-modal information interaction for accurate trajectory regression. Specifically, reasoning tokens provide subjective decision context, occupancy queries impose scene-level constraints,

and ego-state further refines trajectory quality.

4.5. Qualitative Results

We qualitatively visualize representative results of scene understanding and forecasting in Fig. 5. It is evident that SparseOccVLA successfully perceives pedestrians and distant vehicle, which are faithfully reflected in the LLM outputs. It also accurately recognizes red traffic lights and lane markings, benefiting from its fully end-to-end design that enables effective capture of non-geometric visual cues.

5. Conclusion

In this work, we propose SparseOccVLA, which, to the best of our knowledge, is the first to effectively integrate VLMs and occupancy representations, achieving strong performance across understanding, occupancy forecasting, and planning. With only sparse occupancy queries serving as the sole visual bridge to the LLM—without relying on vi-

sual tokens or other perceptual contents—SparseOccVLA establishes a new paradigm beyond MLP-, Q-Former-, and BEV-based alignment strategies that will foster cross-domain research and advances the community.

Limitation Despite its strong performance, SparseOccVLA has several limitations. It relies on dense occupancy supervision, leading to non-trivial construction cost. Moreover, since the closed-loop benchmarks lacks occupancy ground truth, its closed-loop planning capability remains to be further evaluated in future work.

References

- [1] Satanjeev Banerjee and Alon Lavie. Meteor: An automatic metric for mt evaluation with improved correlation with human judgments. In *Proceedings of the acl workshop on intrinsic and extrinsic evaluation measures for machine translation and/or summarization*, pages 65–72, 2005. 5
- [2] Holger Caesar, Varun Bankiti, Alex H Lang, Sourabh Vora, Venice Erin Liang, Qiang Xu, Anush Krishnan, Yu Pan, Giacomo Baldan, and Oscar Beijbom. nuscenes: A multi-modal dataset for autonomous driving. In *Proceedings of the IEEE/CVF conference on computer vision and pattern recognition*, pages 11621–11631, 2020. 5
- [3] Xuesong Chen, Linjiang Huang, Tao Ma, Rongyao Fang, Shaoshuai Shi, and Hongsheng Li. Solve: Synergy of language-vision and end-to-end networks for autonomous driving. In *Proceedings of the Computer Vision and Pattern Recognition Conference*, pages 12068–12077, 2025. 1, 2
- [4] Zhe Chen, Jiannan Wu, Wenhai Wang, Weijie Su, Guo Chen, Sen Xing, Muyan Zhong, Qinglong Zhang, Xizhou Zhu, Lewei Lu, et al. Internvl: Scaling up vision foundation models and aligning for generic visual-linguistic tasks. In *Proceedings of the IEEE/CVF conference on computer vision and pattern recognition*, pages 24185–24198, 2024. 1, 4, 5
- [5] Chenxu Dang, Haiyan Liu, Guangjun Bao, Pei An, Xinyue Tang, Pan An, Jie Ma, Bingchuan Sun, and Yan Wang. Sparseworld: A flexible, adaptive, and efficient 4d occupancy world model powered by sparse and dynamic queries. *arXiv preprint arXiv:2510.17482*, 2025. 2, 3, 6, 4
- [6] Yuxin Fang, Quan Sun, Xinggang Wang, Tiejun Huang, Xinglong Wang, and Yue Cao. Eva-02: A visual representation for neon genesis. *Image and Vision Computing*, 149:105171, 2024. 5
- [7] Haoyu Fu, Diankun Zhang, Zongchuang Zhao, Jianfeng Cui, Dingkang Liang, Chong Zhang, Dingyuan Zhang, Hongwei Xie, Bing Wang, and Xiang Bai. Orion: A holistic end-to-end autonomous driving framework by vision-language instructed action generation. *arXiv preprint arXiv:2503.19755*, 2025. 2
- [8] Songen Gu, Wei Yin, Bu Jin, Xiaoyang Guo, Junming Wang, Haodong Li, Qian Zhang, and Xiaoxiao Long. Dome: Tampering diffusion model into high-fidelity controllable occupancy world model. *arXiv preprint arXiv:2410.10429*, 2024. 2
- [9] Xianda Guo, Ruijun Zhang, Yiqun Duan, Yuhang He, Dujun Nie, Wenke Huang, Chenming Zhang, Shuai Liu, Hao Zhao, and Long Chen. Surds: Benchmarking spatial understanding and reasoning in driving scenarios with vision language models. *arXiv preprint arXiv:2411.13112*, 2024. 1
- [10] Kaiming He, Xiangyu Zhang, Shaoqing Ren, and Jian Sun. Deep residual learning for image recognition. In *Proceedings of the IEEE conference on computer vision and pattern recognition*, pages 770–778, 2016. 5
- [11] Edward J Hu, Yelong Shen, Phillip Wallis, Zeyuan Allen-Zhu, Yuanzhi Li, Shean Wang, Lu Wang, Weizhu Chen, et al. lora. *ICLR*, 1(2):3, 2022. 5
- [12] Yihan Hu, Jiazhi Yang, Li Chen, Keyu Li, Chonghao Sima, Xizhou Zhu, Siqi Chai, Senyao Du, Tianwei Lin, Wenhai Wang, et al. Planning-oriented autonomous driving. In *Proceedings of the IEEE/CVF conference on computer vision and pattern recognition*, pages 17853–17862, 2023. 1, 2, 6
- [13] Zhijian Huang, Tao Tang, Shaoxiang Chen, Sihao Lin, Zequn Jie, Lin Ma, Guangrun Wang, and Xiaodan Liang. Making large language models better planners with reasoning-decision alignment. In *European Conference on Computer Vision*, pages 73–90. Springer, 2024. 2
- [14] Ayesha Ishaq, Jean Lahoud, Ketan More, Omkar Thawakar, Ritesh Thawkar, Dinura Dissanayake, Noor Ahsan, Yuhao Li, Fahad Shahbaz Khan, Hisham Cholakkal, et al. Drivelmm-01: A step-by-step reasoning dataset and large multimodal model for driving scenario understanding. *arXiv preprint arXiv:2503.10621*, 2025. 2
- [15] Xiaosong Jia, Junqi You, Zhiyuan Zhang, and Junchi Yan. Drivetransformer: Unified transformer for scalable end-to-end autonomous driving. *arXiv preprint arXiv:2503.07656*, 2025. 1
- [16] Bo Jiang, Shaoyu Chen, Qing Xu, Bencheng Liao, Jiajie Chen, Helong Zhou, Qian Zhang, Wenyu Liu, Chang Huang, and Xinggang Wang. Vad: Vectorized scene representation for efficient autonomous driving. In *Proceedings of the IEEE/CVF International Conference on Computer Vision*, pages 8340–8350, 2023. 1, 2, 6
- [17] Bo Jiang, Shaoyu Chen, Bencheng Liao, Xingyu Zhang, Wei Yin, Qian Zhang, Chang Huang, Wenyu Liu, and Xinggang Wang. Senna: Bridging large vision-language models and end-to-end autonomous driving. *arXiv preprint arXiv:2410.22313*, 2024. 1, 2
- [18] Junnan Li, Dongxu Li, Caiming Xiong, and Steven Hoi. Blip: Bootstrapping language-image pre-training for unified vision-language understanding and generation. In *International conference on machine learning*, pages 12888–12900. PMLR, 2022. 1, 2
- [19] Junnan Li, Dongxu Li, Silvio Savarese, and Steven Hoi. Blip-2: Bootstrapping language-image pre-training with frozen image encoders and large language models. In *International conference on machine learning*, pages 19730–19742. PMLR, 2023. 1, 2
- [20] Xiang Li, Pengfei Li, Yupeng Zheng, Wei Sun, Yan Wang, and Yilun Chen. Semi-supervised vision-centric 3d occupancy world model for autonomous driving. *arXiv preprint arXiv:2502.07309*, 2025. 2, 5, 6
- [21] Bencheng Liao, Shaoyu Chen, Haoran Yin, Bo Jiang, Cheng Wang, Sixu Yan, Xinbang Zhang, Xiangyu Li, Ying Zhang,

Qian Zhang, et al. Diffusiondrive: Truncated diffusion model for end-to-end autonomous driving. In *Proceedings of the Computer Vision and Pattern Recognition Conference*, pages 12037–12047, 2025. 4, 5

[22] Zhimin Liao, Ping Wei, Ruijie Zhang, Shuaijia Chen, Haoyuan Wang, and Ziyang Ren. i2-world: Intra-inter tokenization for efficient dynamic 4d scene forecasting. *arXiv preprint arXiv:2507.09144*, 2025. 2

[23] Chin-Yew Lin. Rouge: A package for automatic evaluation of summaries. In *Text summarization branches out*, pages 74–81, 2004. 5

[24] Haotian Liu, Chunyuan Li, Qingyang Wu, and Yong Jae Lee. Visual instruction tuning. *Advances in neural information processing systems*, 36:34892–34916, 2023. 1, 2, 6, 3

[25] Haisong Liu, Yao Teng, Tao Lu, Haiguang Wang, and Limin Wang. Sparsebev: High-performance sparse 3d object detection from multi-camera videos. In *Proceedings of the IEEE/CVF international conference on computer vision*, pages 18580–18590, 2023. 3, 2

[26] Haisong Liu, Yang Chen, Haiguang Wang, Zetong Yang, Tianyu Li, Jia Zeng, Li Chen, Hongyang Li, and Limin Wang. Fully sparse 3d occupancy prediction. In *European Conference on Computer Vision*, pages 54–71. Springer, 2024. 1, 2, 3

[27] Ruixun Liu, Lingyu Kong, Derun Li, and Hang Zhao. Oc-cvla: Vision-language-action model with implicit 3d occupancy supervision. *arXiv preprint arXiv:2509.05578*, 2025. 1, 2, 6, 3

[28] Wei Liu, Jiyuan Zhang, Binxiong Zheng, Yufeng Hu, Yingzhan Lin, and Zengfeng Zeng. X-driver: Explainable autonomous driving with vision-language models. *arXiv preprint arXiv:2505.05098*, 2025. 2

[29] Junyi Ma, Xieyuanli Chen, Jiawei Huang, Jingyi Xu, Zhen Luo, Jintao Xu, Weihao Gu, Rui Ai, and Hesheng Wang. Cam4docc: Benchmark for camera-only 4d occupancy forecasting in autonomous driving applications. In *Proceedings of the IEEE/CVF Conference on Computer Vision and Pattern Recognition*, pages 21486–21495, 2024. 2

[30] Qihang Ma, Xin Tan, Yanyun Qu, Lizhuang Ma, Zhizhong Zhang, and Yuan Xie. Cotr: Compact occupancy transformer for vision-based 3d occupancy prediction. In *Proceedings of the IEEE/CVF Conference on Computer Vision and Pattern Recognition*, pages 19936–19945, 2024. 1, 2

[31] Ming Nie, Renyuan Peng, Chunwei Wang, Xinyue Cai, Jianhua Han, Hang Xu, and Li Zhang. Reason2drive: Towards interpretable and chain-based reasoning for autonomous driving. In *European Conference on Computer Vision*, pages 292–308. Springer, 2024. 2

[32] Tianwen Qian, Jingjing Chen, Linhai Zhuo, Yang Jiao, and Yu-Gang Jiang. Nuscenes-qa: A multi-modal visual question answering benchmark for autonomous driving scenario. In *Proceedings of the AAAI Conference on Artificial Intelligence*, pages 4542–4550, 2024. 6, 3

[33] Alec Radford, Jong Wook Kim, Chris Hallacy, Aditya Ramesh, Gabriel Goh, Sandhini Agarwal, Girish Sastry, Amanda Askell, Pamela Mishkin, Jack Clark, et al. Learning transferable visual models from natural language supervision. In *International conference on machine learning*, pages 8748–8763. PMLR, 2021. 1, 4, 5

[34] Chonghao Sima, Katrin Renz, Kashyap Chitta, Li Chen, Hanxue Zhang, Chengen Xie, Jens Beißenwenger, Ping Luo, Andreas Geiger, and Hongyang Li. Drivelm: Driving with graph visual question answering. In *European conference on computer vision*, pages 256–274. Springer, 2024. 2

[35] Jiaming Song, Chenlin Meng, and Stefano Ermon. Denoising diffusion implicit models. *arXiv preprint arXiv:2010.02502*, 2020. 5

[36] Wenchao Sun, Xuewu Lin, Yining Shi, Chuang Zhang, Haoran Wu, and Sifa Zheng. Sparsedrive: End-to-end autonomous driving via sparse scene representation. In *2025 IEEE International Conference on Robotics and Automation (ICRA)*, pages 8795–8801. IEEE, 2025. 1, 2

[37] Xiaoyu Tian, Tao Jiang, Longfei Yun, Yucheng Mao, Huitong Yang, Yue Wang, Yilun Wang, and Hang Zhao. Occ3d: A large-scale 3d occupancy prediction benchmark for autonomous driving. *Advances in Neural Information Processing Systems*, 36:64318–64330, 2023. 5

[38] Xiaoyu Tian, Junru Gu, Bailin Li, Yicheng Liu, Yang Wang, Zhiyong Zhao, Kun Zhan, Peng Jia, Xianpeng Lang, and Hang Zhao. Drivevlm: The convergence of autonomous driving and large vision-language models. *arXiv preprint arXiv:2402.12289*, 2024. 2

[39] Wenwen Tong, Chonghao Sima, Tai Wang, Li Chen, Silei Wu, Hanming Deng, Yi Gu, Lewei Lu, Ping Luo, Dahua Lin, et al. Scene as occupancy. In *Proceedings of the IEEE/CVF International Conference on Computer Vision*, pages 8406–8415, 2023. 1, 2

[40] Aaron Van Den Oord, Oriol Vinyals, et al. Neural discrete representation learning. *Advances in neural information processing systems*, 30, 2017. 1, 2

[41] Ramakrishna Vedantam, C Lawrence Zitnick, and Devi Parikh. Cider: Consensus-based image description evaluation. In *Proceedings of the IEEE conference on computer vision and pattern recognition*, pages 4566–4575, 2015. 5

[42] Jiabao Wang, Zhaojiang Liu, Qiang Meng, Liujiang Yan, Ke Wang, Jie Yang, Wei Liu, Qibin Hou, and Ming-Ming Cheng. Opus: occupancy prediction using a sparse set. *Advances in Neural Information Processing Systems*, 37: 119861–119885, 2024. 2, 3, 4

[43] Peng Wang, Shuai Bai, Sinan Tan, Shijie Wang, Zhihao Fan, Jinze Bai, Keqin Chen, Xuejing Liu, Jialin Wang, Wenbin Ge, et al. Qwen2-vl: Enhancing vision-language model’s perception of the world at any resolution. *arXiv preprint arXiv:2409.12191*, 2024. 1, 2

[44] Shihao Wang, Zhiding Yu, Xiaohui Jiang, Shiyi Lan, Min Shi, Nadine Chang, Jan Kautz, Ying Li, and Jose M Alvarez. Omnidrive: A holistic vision-language dataset for autonomous driving with counterfactual reasoning. In *Proceedings of the Computer Vision and Pattern Recognition Conference*, pages 22442–22452, 2025. 1, 2, 4, 5, 6, 3

[45] Yuqi Wang, Yuntao Chen, Xingyu Liao, Lue Fan, and Zhaoxiang Zhang. Panoocc: Unified occupancy representation for camera-based 3d panoptic segmentation. In *Proceedings of the IEEE/CVF conference on computer vision and pattern recognition*, pages 17158–17168, 2024. 1, 2

[46] Julong Wei, Shanshuai Yuan, Pengfei Li, Qingda Hu, Zhongxue Gan, and Wenchao Ding. Occlama: An occupancy-language-action generative world model for autonomous driving. *arXiv preprint arXiv:2409.03272*, 2024. 1, 2, 6

[47] Jingyi Xu, Xieyuanli Chen, Junyi Ma, Jiawei Huang, Jintao Xu, Yue Wang, and Ling Pei. Spatiotemporal decoupling for efficient vision-based occupancy forecasting. In *Proceedings of the Computer Vision and Pattern Recognition Conference*, pages 22338–22347, 2025. 2

[48] Tianshuo Xu, Hao Lu, Xu Yan, Yingjie Cai, Bingbing Liu, and Yingcong Chen. Occ-llm: Enhancing autonomous driving with occupancy-based large language models. *arXiv preprint arXiv:2502.06419*, 2025. 1, 2, 6

[49] Senqiao Yang, Jiaming Liu, Renrui Zhang, Mingjie Pan, Ziyu Guo, Xiaoqi Li, Zehui Chen, Peng Gao, Hongsheng Li, Yandong Guo, et al. Lidar-llm: Exploring the potential of large language models for 3d lidar understanding. In *Proceedings of the AAAI Conference on Artificial Intelligence*, pages 9247–9255, 2025. 3

[50] Zichen Yu, Changyong Shu, Jiajun Deng, Kangjie Lu, Zongdai Liu, Jiangyong Yu, Dawei Yang, Hui Li, and Yan Chen. Flashocc: Fast and memory-efficient occupancy prediction via channel-to-height plugin. *arXiv preprint arXiv:2311.12058*, 2023. 1, 2

[51] Diankun Zhang, Guoan Wang, Runwen Zhu, Jianbo Zhao, Xiwu Chen, Siyu Zhang, Jiahao Gong, Qibin Zhou, Wenyuan Zhang, Ningzi Wang, et al. Sparsead: Sparse query-centric paradigm for efficient end-to-end autonomous driving. *arXiv preprint arXiv:2404.06892*, 2024. 2

[52] Yunpeng Zhang, Zheng Zhu, and Dalong Du. Occformer: Dual-path transformer for vision-based 3d semantic occupancy prediction. In *Proceedings of the IEEE/CVF International Conference on Computer Vision*, pages 9433–9443, 2023. 2

[53] Zhiyuan Zhang, Xiaofan Li, Zhihao Xu, Wenjie Peng, Zijian Zhou, Miaojing Shi, and Shuangping Huang. Mpdrive: Improving spatial understanding with marker-based prompt learning for autonomous driving. In *Proceedings of the Computer Vision and Pattern Recognition Conference*, pages 12089–12099, 2025. 1

[54] Zongchuang Zhao, Haoyu Fu, Dingkang Liang, Xin Zhou, Dingyuan Zhang, Hongwei Xie, Bing Wang, and Xiang Bai. Extending large vision-language model for diverse interactive tasks in autonomous driving. *arXiv preprint arXiv:2505.08725*, 2025. 2

[55] Lianmin Zheng, Wei-Lin Chiang, Ying Sheng, Siyuan Zhuang, Zhanghao Wu, Yonghao Zhuang, Zi Lin, Zhuohan Li, Dacheng Li, Eric Xing, et al. Judging llm-as-a-judge with mt-bench and chatbot arena. *Advances in neural information processing systems*, 36:46595–46623, 2023. 5, 4

[56] Wenzhao Zheng, Weiliang Chen, Yuanhui Huang, Borui Zhang, Yueqi Duan, and Jiwen Lu. Occworld: Learning a 3d occupancy world model for autonomous driving. In *European conference on computer vision*, pages 55–72. Springer, 2024. 2, 5, 6

[57] Xingcheng Zhou, Xuyuan Han, Feng Yang, Yunpu Ma, and Alois C Knoll. Opendrivevla: Towards end-to-end au-tonomous driving with large vision language action model. *arXiv preprint arXiv:2503.23463*, 2025. 1, 2, 6

[58] Xin Zhou, Dingkang Liang, Sifan Tu, Xiwu Chen, Yikang Ding, Dingyuan Zhang, Feiyang Tan, Hengshuang Zhao, and Xiang Bai. Hermes: A unified self-driving world model for simultaneous 3d scene understanding and generation. *arXiv preprint arXiv:2501.14729*, 2025. 1, 2, 4, 5, 6

SparseOccVLA: Bridging Occupancy and Vision-Language Models via Sparse Queries for Unified 4D Scene Understanding and Planning

Supplementary Material

A. More Details

Model Details To endow SparseOccVLA with dynamic forecasting capability, our Sparse Query Encoder incorporates the Adaptive Scaling in [5] that adjusts the initial query range based on ego states. Each query learns 4 sampling points, which are projected onto and interpolated from the 4-scale feature maps extracted by the visual encoder, followed by the adaptive mixing[25] to consolidate the information. To enhance representational capacity, the occupancy queries are configured with a feature dimension of 1024 and 32 attention heads.

In contrast to standard Multi-Head Self-Attention, the spatially grounded MHSA used in our encoder computes attention weights as follows:

$$A_{ij} = q_i^T q_j - \tau_i \|\mathbf{p}_i - \mathbf{p}_j\|, \quad (9)$$

where $i, j = 1, 2, \dots, N$, p_i index the queries, and τ_i is learned from occupancy query q_i .

Following OmniDrive[44], we also encode the ego state into a single token and feed it to the language model for interpretation. In our anchor-diffusion planner, the hidden feature dimension is aligned with that of the occupancy queries, i.e., $D = 1024$.

Sparse Occupancy Encoder Training To adapt to the occupancy forecasting task, the Adaptive Scaling strategy in [5] is adopted during the training of the Sparse Occupancy Encoder to enlarge the initial query range for dynamic environments. We concatenate the current and future T frames of occupancy ground truth and perform coordinate transformations according to the ego pose to obtain extended-range occupancy supervision.

At each encoding layer, Chamfer Distance loss is employed for geometric supervision, while Focal loss provides semantic supervision, jointly guiding the model learning process. The overall training objective of the Sparse Occupancy Encoder is defined as follows:

$$\mathcal{L}_{\text{occ}} = \sum_{l=0}^L \mathcal{L}_{\text{CD}}(\mathcal{P}_l, \mathcal{G}) + \sum_{l=1}^L \lambda_{\text{focal}} \mathcal{L}_{\text{focal}}(C_l, \hat{C}_l) + \mathcal{L}_{\text{distill}}, \quad (10)$$

where $\mathcal{L}_{\text{CD}}(\mathcal{P}_0, \mathcal{G})$ denotes that the geometric supervision is also applied to the original point set \mathcal{P}_0 . C_l and \hat{C}_l represent the predicted point classes and their corresponding ground truth labels at layer l , respectively. The weighting factor λ_{focal} is set to 0.2.

End to End Training During the end-to-end training phase, all modules are jointly optimized. The occupancy forecasting is supervised on a per-frame basis. Unlike [5], we utilize the concatenated occupancy ground truth \mathcal{G} as the base and transform the supervision to the corresponding future frames according to expert trajectories using the vehicle pose matrices. The overall occupancy prediction loss is computed as follows:

$$\mathcal{L}_{\text{fore}} = \sum_{t=1}^T \mathcal{L}_{\text{CD}}(\mathcal{P}_t, \mathcal{G}_t) + \sum_{t=1}^T \lambda_{\text{focal}} \mathcal{L}_{\text{focal}}(C_t, \hat{C}_t), \quad (11)$$

where T denotes the number of predicted frames, and $\mathcal{P}_t, \mathcal{G}_t, C_t, \hat{C}_t$ represent the predicted point set, the transformed ground truth, the predicted point classes, and the corresponding ground truth labels at time step t , respectively.

The total training objective consists of four components, namely the occupancy perception loss, the language modeling loss, the occupancy prediction loss, and the trajectory noise prediction loss:

$$\mathcal{L}_{\text{total}} = \mathcal{L}_{\text{occ}} + \mathcal{L}_{\text{LM}} + \mathcal{L}_{\text{fore}} + \mathcal{L}_{\text{diff}} \quad (12)$$

B. More Analysis

In this section, we analyze the significance of SparseOccVLA to the autonomous driving community and explain why we regard it as the first effective integration of vision-language models and semantic occupancy.

As discussed in the main text, both paradigms have achieved remarkable progress in recent years—VLMs excel in high-level reasoning, while occupancy representations provide precise, fine-grained spatial understanding. Combining these two paradigms is naturally appealing, as they possess complementary strengths. However, this integration is highly challenging due to the severe cross-modal gap and computational inefficiency. Occupancy features are dense and low-level, while language tokens are sparse and abstract, making alignment inherently difficult. Regarding the role of occupancy in Vision-Language Models (VLMs), we categorize existing methods into three types, as illustrated in Fig. 6.

As illustrated in Fig. 6(a), early explorations[46, 48] attempted to embed occupancy ground truth via a VAE before feeding it into a large language model. Although alleviating computational cost, it completely decouples upstream perception from downstream reasoning. Consequently, the

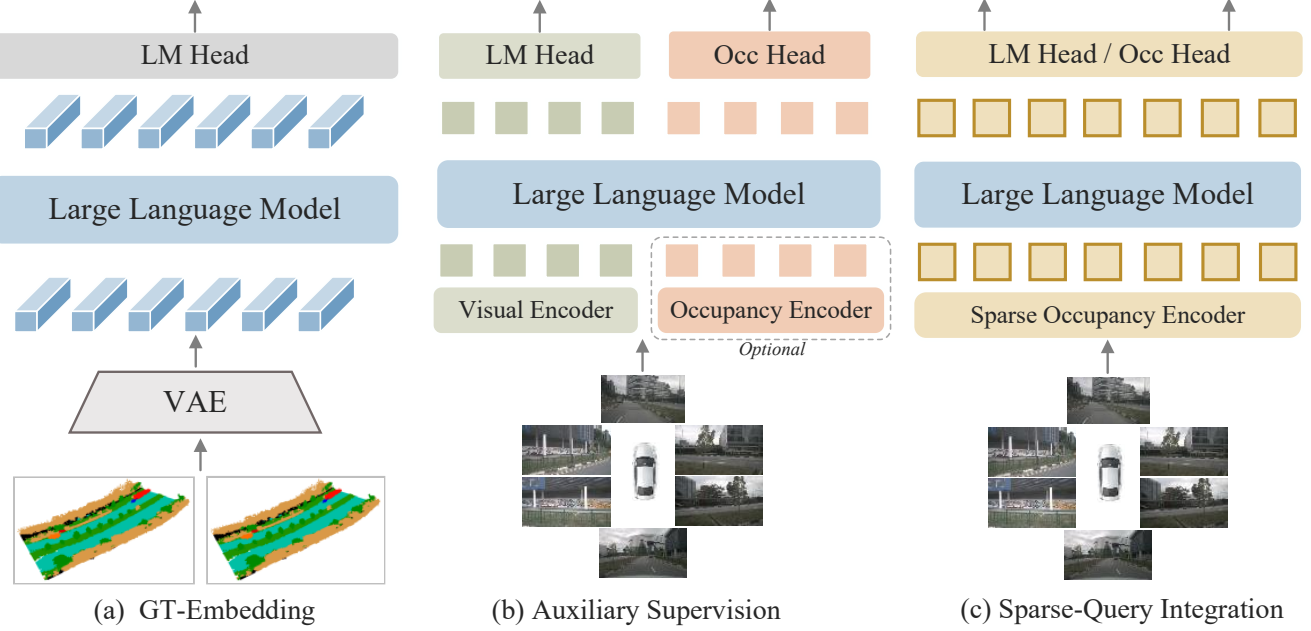


Figure 6. Comparison of different occupancy-VLM integration paradigms.

LLM only observes geometrically defined elements while discarding critical non-geometric cues such as traffic lights, lane markings, and signs, which limit the model’s upper bound. This design violates the principle of end-to-end autonomous driving and has not been widely recognized.

More recent works[27], shown in Fig. 6(b), introduce an auxiliary occupancy encoder alongside the vision encoder for additional supervision. However, such designs still depend on visual tokens and thus suffer from the same limitations as conventional VLMs. In these methods, occupancy plays only a marginal role rather than fundamentally departing from the established VLM paradigm.

In contrast, SparseOccVLA (Fig. 6(c)) introduces a sparse occupancy encoder that extracts sparse occupancy queries serving as the sole bridge between vision and language, completely eliminating the dependency on any visual tokens.

These sparse occupancy queries offer three key advantages:

- **Compact:** leveraging the efficiency of sparse-based occupancy prediction. In our implementation, only 300 tokens are required to achieve outstanding scene understanding performance.
- **Information rich:** preserving dense geometric and semantic cues from raw visual inputs, aligning with the principle of end-to-end modeling.
- **Modeling friendly:** possessing explicit spatial attributes that enable flexible temporal fusion, enhancing spatial reasoning and interpretability.

In summary, SparseOccVLA effectively resolves long-

Table 5. Comparison of different methods on nuScenes-QA benchmark.

Method	Reference	Input	Acc.(%) \uparrow
LLaVA[24]	NeurIPS 23	Image	47.4
LiDAR-LLM[49]	AAAI 25	LiDAR	48.6
BEVDet+MCAN[32]	AAAI 24	Image	57.9
CenterPoint+MCAN[32]	AAAI 24	LiDAR	59.5
OmniDrive[44]	CVPR 25	Image	59.2
SparseOccVLA	Ours	Image	60.8

standing issues of information loss, external dependency, and computational inefficiency, achieving a truly unified framework that combines the complementary advantages of occupancy and VLMs in a principled and efficient manner.

C. More Experiments

C.1. Results on nuScenes-QA

Following previous works[44], we conduct experiments on the nuScenes-QA[32] dataset to demonstrate the generalization capability of SparseOccVLA. nuScenes-QA is another widely used visual question answering (VQA) benchmark. Unlike OmniDrive-nuScenes[44], which mainly contains long-form textual answers, the answers in nuScenes-QA are mostly short and deterministic words. As shown in Tab. 5, SparseOccVLA also achieves an accuracy of 60.8%, significantly surpassing the existing state-of-the-art methods.

C.2. More Ablation Results

In this section, we provide additional ablation studies to illustrate the detailed design of our model and help readers gain a deeper understanding of our approach.

Table 6. Ablation study on the effect of normalization layer. We report the mIoU perceptual score of the current frame, which reflect the learning effectiveness of the Sparse Occupancy Encoder.

Distill	Norm	mIoU	CIDEr	METEOR	ROUGE
✗	✗	17.68	0.776	0.376	0.329
✓	✗	15.43	0.743	0.372	0.324
✓	✓	17.65	0.792	0.384	0.334

Effect of Normalization Layers As shown in Tab. 6, we present the ablation study on the effect of the normalization layer. When the Norm Layer is removed, the mIoU of the current frame drops significantly compared to the setting with the Norm Layer, which further degrades the language understanding metrics. We attribute this to the overly strong distillation loss that enforces the occupancy features to be directly aligned with the full language space, leading to gradient conflicts and hindering the learning of the Sparse Occupancy Encoder. In contrast, the Norm Layer effectively alleviates this issue by enabling smoother feature alignment without imposing excessive fine-grained constraints. Comparing the 2nd and 4th rows, together with other ablations in the main text, we observe that the Norm Layer greatly improves training stability and convergence speed while maintaining the perception capability of the occupancy encoder.

Table 7. Effect of different numbers of global queries on various language metrics.

Global Query	CIDEr	METEOR	ROUGE
0	0.758	0.378	0.327
4	0.775	0.381	0.330
8	0.786	0.383	0.332
12	0.792	0.384	0.333
16	0.793	0.384	0.334

Effect of the Number of Global Queries Tab. 7 presents an analysis of SparseOccVLA’s sensitivity to the number of global queries. Overall, increasing the number of global queries significantly enhances the model’s understanding capabilities, exhibiting a clear scaling trend. Performance saturates when the number of global queries exceeds 12, but no degradation is observed. This observation supports our hypothesis: while sparse occupancy queries focus primarily

on local details, global queries attend to and integrate information from all queries, thereby facilitating the LLM’s comprehension of the entire scene.

Table 8. Impact of the number of input image frames on understanding and prediction performance of SparseOccVLA.

Frames	Understanding			mIoU	
	CIDEr	METEOR	ROUGE	Curr	Fut.avg
1	0.742	0.381	0.326	16.52	12.60
2	0.759	0.385	0.30	16.97	13.02
4	0.776	0.387	0.331	17.38	13.31
8	0.792	0.388	0.334	17.65	13.53

Effect of the Image Frames SparseOccVLA inherits the advantages of the Sparse Occupancy Encoder, enabling it to attend to historical image frames in parallel and thereby exhibiting flexible and powerful temporal modeling capabilities. In Table 4, we investigate the impact of the number of input image frames on both understanding and prediction performance. We observe a positive correlation between the number of input frames and the performance in scene understanding as well as occupancy perception and forecasting, reflecting the model’s scalability. Notably, lower-level mIoU metrics demonstrate higher sensitivity to the number of frames. Traditional vision-language models struggle to process video streams, which limits the language model’s ability to capture temporal dynamics and constrains the overall performance ceiling. We also observe that even with a single input frame, although performance is significantly reduced, SparseOccVLA still performs comparably to the baseline HERMES[58] model, demonstrating the potential of sparse occupancy queries to replace BEV representations.

Effect of Occupancy Query Dimension In Tab. 9, we investigate the influence of the occupancy-query feature dimension D . Notably, D is decoupled from both the image encoder and the LLM, allowing it to be flexibly adjusted. Unlike precedent works[5, 42] that typically fixes $D = 256$, our early experiments indicate that such a low-dimensional setting leads to suboptimal semantic understanding. As shown in Tab. 9, increasing the occupancy-query dimension from 256 to 1024—while keeping all other hyperparameters unchanged—consistently improves performance. This trend demonstrates the scalability of our model.

Experiments of other LLMs To ensure comprehensive comparison with existing methods and to assess the generalization of SparseOccVLA, we replace Vicuna[55] with InternVL2[4] and retrain as well as reevaluate the

Table 9. Effect of the occupancy query feature dimension D on model performance.

Feature Dim (D)	CIDEr	METEOR	ROUGH
256	0.761	0.375	0.327
512	0.779	0.383	0.332
1024	0.792	0.388	0.334

Table 10. Comparison of language metrics across different model sizes.

Model	LLM	CIDEr	METEOR	ROUGE
HERMES	InternVL2-2B	0.377	0.321	0.740
Ours	InternVL2-2B	0.386	0.335	0.785
HERMES	InternVL2-4B	0.381	0.325	0.747
Ours	InternVL2-4B	0.388	0.338	0.797

Table 11. Effect of denoising steps and anchor numbers on planner performance.

Denoising	Anchor	L2 Error (m)			
		1s	2s	3s	Avg
1	18	0.145	0.237	0.332	0.238
2	18	0.141	0.224	0.298	0.221
3	18	0.140	0.224	0.300	0.221
2	15	0.146	0.247	0.348	0.247
2	21	0.142	0.229	0.313	0.228

model. In our implementation, the visual encoder of InternVL is frozen and substituted with our sparse occupancy query. As shown in the Tab. 10, under the same parameter budget, SparseOccVLA consistently outperforms HERMES[58] across language metrics, further demonstrating the effectiveness of the proposed sparse occupancy query design.

Comparison of Anchor Number and Denoising Steps In Tab. 11, we analyze the sensitivity of SparseOccVLA’s planning metrics with respect to the number of denoising steps and the number of anchors. The results show that the model is relatively robust to the number of denoising steps: only two denoising steps are sufficient to achieve the best performance, and additional steps do not yield further improvements. In contrast, SparseOccVLA is more sensitive to the number of anchors. Following the design of DiffusionDrive[21], we observe that generating six anchors per direction—resulting in a total of 18 anchors—produces the highest planning scores. We attribute this trend to the fact that too few anchors fail to adequately cover the entire scene, while too many anchors introduce mutual interference.

Table 12. Detailed Comparison of model configurations with vision components.

Model	Vision	Token	Image-Size
OmniDrive[44]	EVA-02-L[6]	513	640 × 640
HERMES[58]	OpenCLIP[33]	2500	1600 × 900
SparseOccVLA	ResNet-50	612	256 × 704

Table 13. Comparison of training efficiency and hardware usage.

Model	Device	Epoch	Time	Memory
HERMES[58]	H20 × 32	36	26h	80G
SparseOccVLA	H20 × 8	12	11h	45G

D. Efficiency Comparison

In this section, we provide a detailed analysis of the training and inference efficiency of SparseOccVLA, and compare it against state-of-the-art methods.

Model Analysis As shown in the Tab. 12, we compare SparseOccVLA with other models in terms of parameters outside the language model. Our visual backbone uses the lightweight ResNet-50[10] to preserve perception-level details. Moreover, the input image resolution is significantly lower than that of OmniDrive and HERMES. Such a lightweight perception module directly contributes to improved training and inference efficiency. We provide a detailed analysis in the following.

Training Efficiency As shown in Tab. 13, we compare the training resources required by HERMES[58] and our SparseOccVLA, where both methods utilize InternVL2-2B[4] as the language model and adopt the official default settings for all other components. We observe that SparseOccVLA is highly efficient: it converges within only 12 epochs using 8 H20 GPUs, with a total training time less than half of HERMES and a peak memory usage slightly above half of it. This efficiency primarily stems from SparseOccVLA’s lightweight visual encoder and its highly compact token representation.

E. More Qualitative results

In Fig. 7, Fig. 8, and Fig. 9, we present additional visualization results of SparseOccVLA’s understanding and forecasting capabilities. The analysis reveals that SparseOccVLA not only reconstructs driving scenes effectively and comprehends the environment in textual form, but also performs deep reasoning and analysis, demonstrating its powerful multimodal abilities. These visualizations also highlight its ability to anticipate future interactions.



Q1: What can you observe from the provided images regarding the driving conditions?

A1: The vehicle is positioned on a quiet, tree-lined road with a pedestrian crossing ahead. To the left, a pedestrian is walking along the sidewalk, while another pedestrian is seen crossing the road at the designated crossing. The road ahead is clear, with no immediate traffic, and a pedestrian is seen walking on the sidewalk to the right. The weather appears overcast, suggesting it might be early morning or late afternoon. The surrounding area is a mix of residential and commercial buildings, with a blue car visible on the left side. Looking behind, the road is also clear with no following traffic, and a pedestrian is seen walking on the sidewalk to the right, indicating a peaceful driving environment.

Q2: How would you describe the pedestrian activity near the vehicle?

A2: There is a pedestrian walking on the sidewalk to the left of the vehicle, and another pedestrian is seen walking on the sidewalk to the right.

Q3: Are there any road signs or directions visible?

A3: Yes, there is a road sign indicating a left turn ahead on the right side of the road.

Q4: What types of vehicles can be seen around you?

A4: There are various types of vehicles including a blue car driving along the road on the left side of the road and a few cars stopping nearby.

Q5: Based on the setting, what can you infer about the speed limit or driving behavior expected here?

A5: Given the residential setting with pedestrian crossings and a single lane road, it is likely that the speed limit is moderate and that drivers are expected to be cautious and attentive to pedestrian activity.

Q6: Can you identify any safety measures in the area for pedestrians?

A6: Yes, there are zebra crossings at the intersection to the left, which provide a safe crossing point for pedestrians.

Q7: Considering the overcast weather, what adjustments should the driver make?

A7: The driver should ensure the vehicle's lights are on for better visibility and be prepared for potentially slick road conditions if it starts to rain.

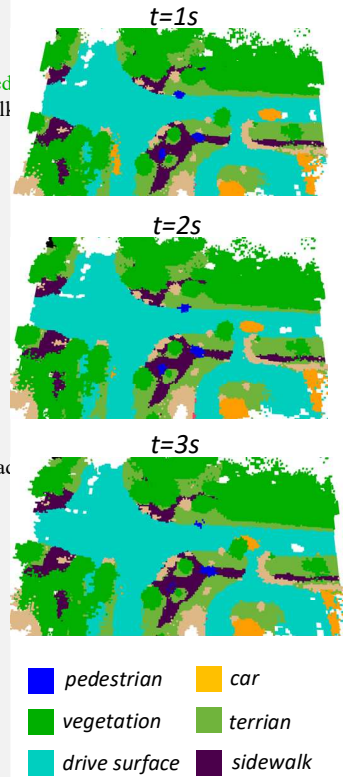


Figure 7. A visualization of reasoning results in an intersection scenario.



Q1: Could you summarize the current driving conditions based on the input images?

A1: The vehicle is positioned on a **multi-lane road** during what appears to be daytime with clear weather conditions. To the left, the road is bordered by a sidewalk and a fence, beyond which lies a grassy area and a building with a modern facade. Directly ahead, **the road is marked with clear lane lines and a few vehicles are visible**, maintaining a **steady flow of traffic**. The right side shows a similar urban setting with buildings and a **pedestrian crossing**. In the rear view, the road is similarly bordered by a fence on the left and buildings on the right, **with no vehicles directly behind**, suggesting a relatively light traffic condition.

Q2: What is the make and color of the car to the front-left of our vehicle?

A2: The car to the front-left is a **silver sedan**.

Q3: Is there a bicycle lane visible, and if so, are there any cyclists currently using it?

A3: Yes, there is a **bicycle lane visible on the left side of the road**, but there are **no cyclists currently using it**.

Q4: What types of vehicles can be seen around you?

A4: There are various types of vehicles including a **blue car driving along the road on the left side** of the road and **a few cars stopping nearby**.

Q5: Is the road we are on showing any signs of congestion?

A5: No, the road ahead is **clear with no signs of congestion**.

Q6: Considering the road conditions and the buildings around, can you infer the type of area we are driving through?

A6: Given the presence of modern buildings, a well-maintained road, and a fenced-off area, it seems we are driving through a **developed urban area**, possibly a business district or a residential area with commercial properties.

Q7: Given the weather and road conditions, what would be the best driving practices to follow right now?

A7: Given the overcast weather and wet road conditions, the best driving practices would be to maintain a moderate speed, keep a safe distance from the vehicle ahead, use headlights for better visibility, and be extra vigilant for any sudden movements from other vehicles or pedestrians.

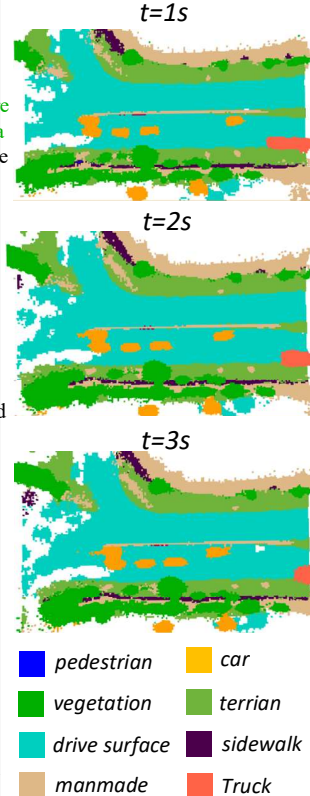


Figure 8. A visualization of reasoning results in an urban road scenario.



Q1: Could you summarize the current driving conditions based on the input images?

A1: The vehicle is positioned on a **two-lane road flanked by urban infrastructure**. To the left, a **pedestrian pathway runs parallel to the road**, bordered by a metal **fence** and lush **greenery**, with a **pedestrian** walking along the path. Directly ahead, the road is clear with no immediate **obstructions**, and a few **vehicles** are visible in the distance, suggesting light traffic conditions. To the right, a **bus stop** is occupied by a few **waiting passengers**, indicating a functional public **transport system** in the area. The sky is overcast, suggesting it might be early morning or late afternoon. Looking behind, the road remains clear with no vehicles in close proximity, and the **environment** mirrors the front with **urban buildings** and **pedestrian walkways**.

Q2: What type of area is the vehicle driving through?

A2: The vehicle is driving through an **urban area** with a **bus stop**, a mix of **commercial** and **residential buildings**.

Q3: Is there any indication of construction or road work in the area?

A3: There is **no visible indication of construction** or road work in the immediate area around the vehicle.

Q4: What types of vehicles can be seen around you?

A4: There are various types of vehicles including a **blue car** driving along the road on the left side of the road and a few cars stopping nearby.

Q5: What instructions would the solid yellow center line on the road give to the driver?

A5: The solid yellow center line indicates that the driver **should not cross over into the opposite lane**, as it is a no-passing zone.

Q6: What should the driver be cautious of near the bus stops?

A6: The driver should be cautious of **pedestrians** who may step onto the road unexpectedly, especially near the bus stops where people are waiting.

Q7: How does the environment suggest the functionality of the public transport system?

A7: The presence of a **bus stop** and a **bus on the road** suggests that the public transport system is **operational** and likely facilitates the movement of people within the area.

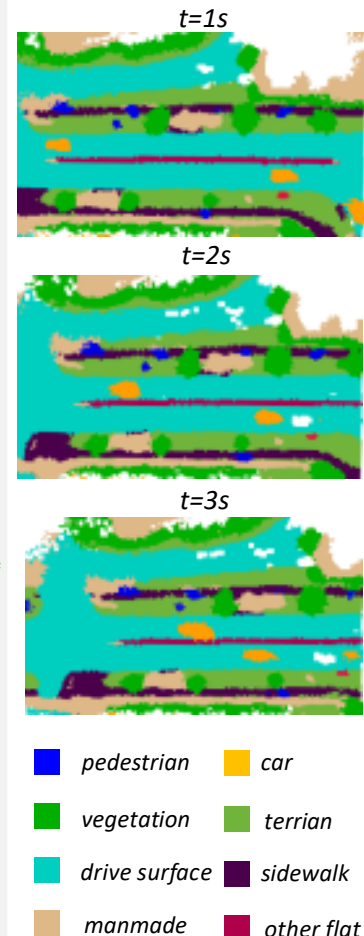


Figure 9. A visualization of reasoning results in an urban road scenario.